Journal of Building Performance Simulation

ISSN: (Print) (Online) Journal homepage: www.tandfonline.com/journals/tbps20

# Thermally anisotropic building envelope for thermal management: finite element model calibration using field evaluation data

Daniel Howard, Som S. Shrestha, Zhenglai Shen, Tianli Feng & Diana Hun

**To cite this article:** Daniel Howard, Som S. Shrestha, Zhenglai Shen, Tianli Feng & Diana Hun (20 Sep 2024): Thermally anisotropic building envelope for thermal management: finite element model calibration using field evaluation data, Journal of Building Performance Simulation, DOI: 10.1080/19401493.2024.2404638

**To link to this article:** https://doi.org/10.1080/19401493.2024.2404638

Published online: 20 Sep 2024.

JOURNAL OF BUILDING PERFORMANCE SIMULATION
https://doi.org/10.1080/19401493.2024.2404638



# Thermally anisotropic building envelope for thermal management: finite element model calibration using field evaluation data

Daniel Howard[a], Som S. Shrestha[a], Zhenglai Shen[a], Tianli Feng[b] and Diana Hun[a]

[a]Buildings and Transportation Science Division, Oak Ridge National Laboratory, Oak Ridge, TN, USA; [b]Department of Mechanical Engineering, University of Utah, Salt Lake City, Utah, USA

**ABSTRACT**

The thermally anisotropic building envelope (TABE) is an active building envelope that redistributes thermal loads in response to weather conditions and building energy demand. Conductive layers throughout the TABE distribute low-grade heat among hydronic loops, altering heat flow direction and intensity. Finite element models of TABE roof and wall panels were developed and calibrated using field evaluation data. The calibration results showed that heat flux differences between the experimental data and finite element models averaged −0.42% and 3.57%, with a maximum mean square error of 1.78 and 3.96 for roof and wall panels, respectively. A reduction in heat flux from the environment to the building living space over the entire testing period (weeks in July/August) was found to be 85% for roof panels and 335% (load reversed) for wall panels. These results indicate TABE can effectively harness low-grade thermal energy sources to achieve high energy efficiency and promote demand-side management.

**ARTICLE HISTORY**
Received 3 April 2024
Accepted 9 September 2024

**KEYWORDS**
Thermally anisotropic building envelope; active building envelope; thermal management; energy efficiency; finite element model calibration

## 1. Introduction

Thermal management is of paramount importance in reducing energy consumption and associated $CO_2$ emissions in buildings, which account for nearly 40% of total energy use and 30% of total $CO_2$ emissions in the world (Yang, Yan, and Lam 2014). Heating, ventilation, and air conditioning (HVAC) energy savings can be realized by proper thermal management of the building envelope without compromising thermal comfort (Bhamare, Rathod, and Banerjee 2019; Sadineni, Madala, and Boehm 2011; Yang, Yan, and Lam 2014). The appropriate balance between energy savings and thermal comfort in buildings is critical to developing sustainable cities. In buildings, thermal management involves the regulation of transient heating and cooling loads to achieve a desired HVAC energy profile. Thermal management in buildings has been explored with both envelope- and equipment-based approaches. However, further research is needed to move beyond the current state of the art in building energy performance. The objective of this paper is to demonstrate building envelope thermal management using the thermally anisotropic building envelope (TABE) through field evaluation and calibrated finite element (FE) models.

Numerous methods have been explored as potential solutions to tackle the challenge of building envelope thermal management. Thermally insulative materials have traditionally been used as the primary means of reducing unwanted heat flow through the opaque building envelope. Increases in thermal insulation have diminishing returns and can, in certain cases, have a negative effect on the energy performance of a building (Kosny et al. 2010). In most climate zones, there are times when increased contact with environmental conditions would be favourable toward maintaining the desired indoor temperature. For instance, during summer months, a building may still be very warm when the outdoor temperature falls in the evening; therefore, having less thermal insulation would be beneficial to allow heat exchange between the indoors and outdoors. This highlights the importance of a dynamically adaptable envelope integrated with an advanced control strategy. A few other explored methods include phase change materials (PCMs), high thermal mass, solar control and shading, and ventilation (Bhamare, Rathod, and Banerjee 2019; Kosny et al. 2014; Sadineni, Madala, and Boehm 2011). However, high cost, low durability, and lack of large-scale studies in real building applications have raised doubts about

**CONTACT** Som S. Shrestha shresthass@ornl.gov Buildings and Transportation Science Division, Oak Ridge National Laboratory, 37831, Oak Ridge, TN, USA

high-performance building insulation materials and passively controlled PCM as effective solutions for building envelope thermal management (Baetens et al. 2010; Baetens, Jelle, and Gustavsen 2011; Biswas 2018; Biswas et al. 2018; Kosny et al. 2014).

Thermal energy storage (TES) has immense potential for redistributing energy in response to demand. Although several methods have been explored to embed phase change materials (a type of TES) within the building envelope, a lack of active control has prevented these previous studies from fully realizing the potential for efficient collection and redistribution of thermal energy (Carpenter et al. 2014; Elnaijar 2017; Lakhdari, Chikh, and Campo 2020; Pasupathy and Velraj 2008; Saffari, Roe, and Finn 2022). Actively controlled TES integrated with HVAC and other residential and industrial equipment has also been explored (Hirmiz et al. 2019; Tarumi, Fujii, and Ito 1991). Some of these concepts show significant energy savings potential. The recently developed TABE harnesses the benefits of active thermal management integrated with the building envelope, thus allowing envelope-based thermal management systems to reach equal or greater widespread impact when compared with equipment-integrated thermal management systems.

At the US Department of Energy's Oak Ridge National Laboratory (ORNL), researchers Som Shrestha and Kaushik Biswas proposed a TABE, an effective thermal management method for building envelopes (Biswas et al. 2019). They demonstrated that the TABE is a promising technology for reducing peak heat gains/losses and overall heat transfer when compared with insulative-only measures. In contrast to typical building envelope constructions, TABE uses conductive metal layers embedded in building envelopes in conjunction with a hydronic piping network to create a thermally anisotropic construction that redirects heat transfer from out-of-plane to in-plane. The TABE design was inspired by techniques used for heat dissipation and hot spot remediation in electronics (Cometto et al. 2017; Huang et al. 2016; Ren and Lee 2018; Suszko and El-Genk 2016; Termentzidis 2018). In the work of Biswas et al. (2019), the thermal anisotropy was accomplished by alternate layers of polyisocyanurate foam board (polyiso) with thin aluminum foils connected to hydronic loops. These highly conductive aluminum foils redirected heat along the building envelope to heat sinks composed of hydronic loops. By selective control of the fluid flow rate and temperature, the magnitude of redirected heat flux can be dynamically controlled as dictated by the thermal loads imposed on the envelope.

The TABE is similar in some aspects to a typical hydronic heating/cooling system (Mokhtari, Ulpiani, and Ghasempour 2022; Xing and Li 2022). Like a typical hydronic system, TABE uses a fluid flowing through piping to provide radiant heating or cooling. Additionally, TABE can be tailored to boost the insulative properties of a building envelope. This is accomplished by preventing a significant portion of heat or coolness from passing through the building envelope owing to redirection of heat along the aluminum foil layers. One key advantage of TABE over typical hydronic systems is the utilization of a thermally anisotropic construction, which allow a much larger spacing between the individual hydronic loops than what would normally be possible for desired performance. Whereas typical hydronic systems require loop spacing of several inches, thermally anisotropic construction of TABE can allow the spacing between loops to be increased to 16 in. or more. This leads to a significant decrease in material and construction costs associated with the fabrication of panels containing TABE, compared with the costs of other hydronic systems.

To verify the TABE system's potential, field evaluations, numerical parameter studies using calibrated models, and whole-building energy simulations in multiple climate zones were all required. The calibration of FE models with field evaluation data was of high importance in quantifying building energy performance. Owing to the small scale of the field evaluation TABE panels, only heat flux data could be collected. FE modelling was required to analyze the heat flux effect and to scale this heat flux up to predict the whole building's thermal load and energy savings. Additionally, the calibrated TABE FE models provide immense flexibility in determining the optimal water flow rate and control strategy for different operation cases in various climate zones.

This study focuses on the field evaluations and FE modelling of TABE panels to quantify the thermal load reduction potential. First, field evaluations were conducted in two test sites—Oak Ridge, Tennessee, and Charleston, South Carolina—for the TABE roofs and walls, respectively. Subsequently, FE models were developed in COMSOL multiphysics and calibrated by using field evaluation data. The FE calibration included the adjustment of convergence tolerance, hydronic loop convection, and sensor locations. Accuracy was quantified as the average error and maximum mean square error for each test period. The thermal performance of TABE panels was then assessed relative to the panels' cooling thermal load reduction under different operating conditions.

## 2. Methods

### 2.1. Experimental design

The field evaluations were conducted at two locations—Oak Ridge, Tennessee, and Charleston, South Carolina. In the Oak Ridge field testing, TABE roof panels


**Figure 1.** Field installation of TABE roof panels at the RTRA in Oak Ridge: (a) lifting panels into place and (b) after installation; and (c) exterior of the RTRA test facility.

were designed and installed in a roof thermal research apparatus (RTRA). A baseline roof panel was prepared without thermal anisotropy, and two TABE roof panels were prepared with different arrangements of thermal anisotropy (A1 and A2). In Charleston, TABE wall panels were built and installed in a natural exposure test (NET) facility. Similarly, a baseline wall panel was prepared without thermal anisotropy, and three TABE wall panels were prepared with different arrangements of thermal anisotropy (A1, A2, and A3). In both locations, the buildings were unoccupied and exposed to natural weather conditions. The TABE test sites with installed TABE roof and wall panels are presented in Figures 1 and 2.

FE models were developed to simulate TABE performance and were calibrated against experimental data collected from the two test sites. The development of FE models primarily served two purposes. First, developing TABE FE models alongside the collection of experimental data allows for a sanity check to identify potential errors in the complex experimental data collection configuration. The temperature predicted by the FE models between each material layer could be compared with that obtained from the experimental setup to determine if potential sensory or calibration concerns were present. Second, because the TABE panels were installed only in small portions of the building envelope, energy savings potential could not be directly measured. Therefore, only thermal load savings through each panel in the form of heat flux could be obtained. Calibrated FE models enable scaling up these thermal load savings to predict whole-building energy savings. The calibrated FE models could also be used to extrapolate energy consumption to various climate zones.

### *2.1.1. Experiment setup and instrumentation*

The experimental setup at the RTRA was designed to evaluate the performance of the TABE in a commercial building roof application. The setup included three roof panels (a baseline and two panels with TABEs). The panel assemblies consisted of an ethylene propylene diene terpolymer (EPDM) roofing membrane as the outermost layer.


**Figure 2.** Field installation of TABE wall panels at the Charleston NET facility: (a) panel preparation and (b) panel installation; and (c) exterior of the NET facility.

Directly below this layer, two layers of 0.5 in. (1.3 cm) polyiso were installed, followed by one layer of 3 in. (7.6 cm) polyiso, one layer of 0.5 in. (1.3 cm) wood fibreboard, and last, a metal decking. Figure 3 shows layering of the materials in the panel formation.

The first roof panel containing TABEs (A1) used three layers of nonperforated aluminum foil. The foil layers were 10 mils (0.254 mm) thick and were mounted above each layer of polyiso. To achieve heat conduction along the TABE panel to the heat sink, these aluminum foils were connected to a hydronic tubing network. The copper tubes used were 0.5 in. (1.27 cm) in diameter and were connected to the aluminum foils using copper taping with conductive adhesive.

The second roof panel containing TABEs (A2) used two hydronic loop systems (an interior and an exterior hydronic loop). The exterior hydronic loop was connected to three layers of perforated aluminum foil. The choice for perforated foils was made for this panel to assess if the perforations were necessary to maintain moisture migration through the building envelope. As before, the foils chosen were 10 mils (0.254 mm) thick and were mounted above each polyiso layer. An additional fourth nonperforated aluminum foil layer was added above the wood fibreboard layer to provide heat redirection specific to the interior hydronic loop. Each of these four aluminum foil layers was again connected to 0.5 in. (1.27 cm) copper tubing via copper tape with conductive adhesive. By connecting the outer three foils to a separate hydronic loop from the interior foil layer, the design allowed the use of only the exterior hydronic loop or only the interior hydronic loop. All panel assemblies met ASHRAE 90.1-2010 R-value requirements for commercial building roofs in climate zone 4.

Ten heat flux transducers (HFTs) and 40 type T thermocouples were installed to monitor heat flux and temperature distribution at various locations. Two HFTs were mounted at the centre of the panels, one on top and one on the bottom of the wood fibreboard. The HFT mounted on the bottom of the wood fibreboard (on top of the metal deck) represented the heat flow between the roof and indoor air. Because of the potential high

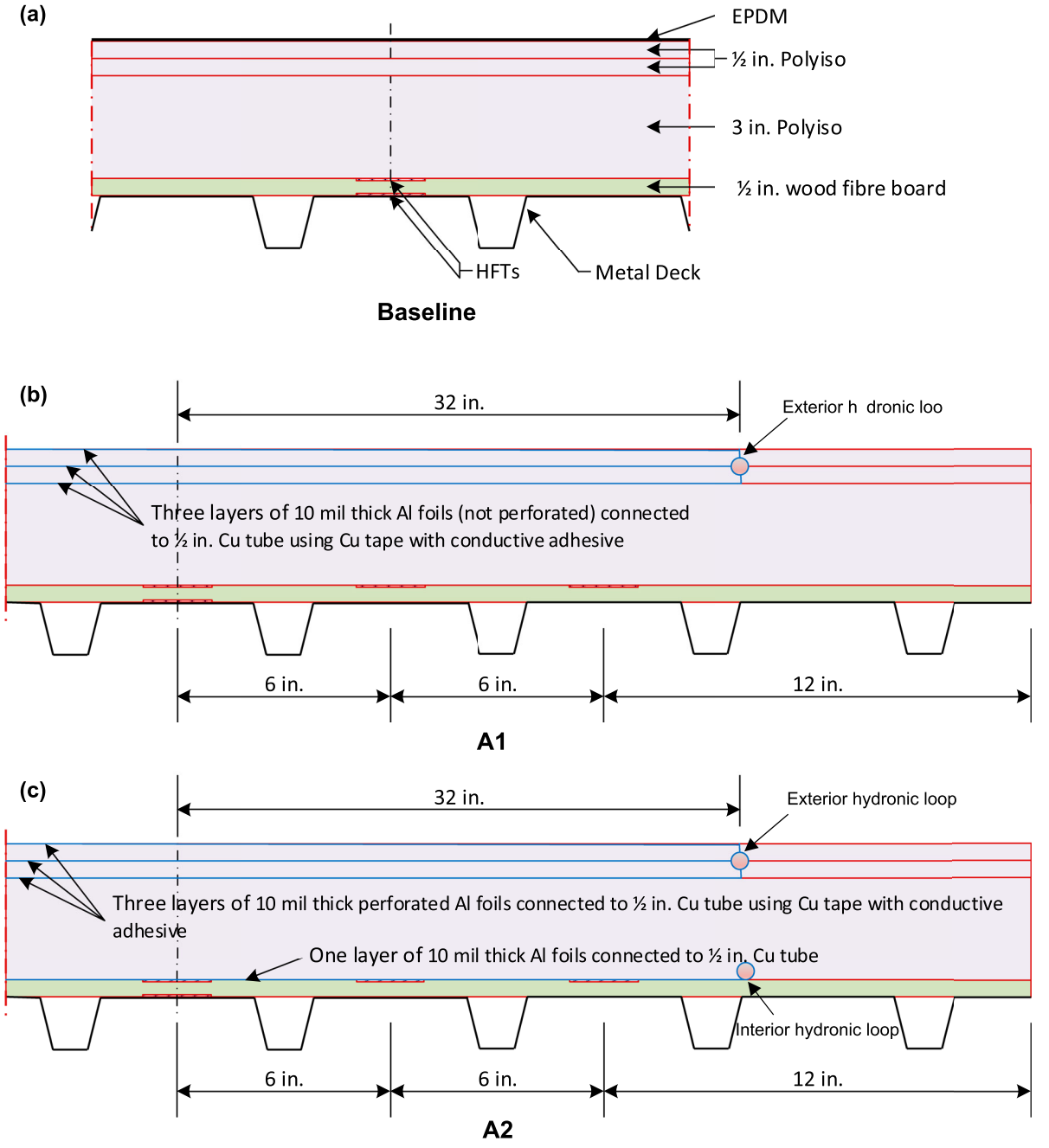


**Figure 3.** Cross sections of the TABE panels installed at the RTRA: (a) baseline, (b) A1, and (c) A2. Heat flux transducers (HFTs) 1, 2, 3, and 4 are numbered counterclockwise starting at the lower HFT.

noise that can cause a low signal-to-noise ratio when installing HFTs on metal surfaces and on top of the metal deck, a set of HFTs was also installed on top of the wood fibreboard.

The HFTs were calibrated using ORNL's heat flow metre apparatus. Water temperatures at the inlet and outlet of each hydronic loop, as well as the water flow rate for each hydronic loop, were recorded. In addition, a weather station was installed at the RTRA to collect local weather data to be used as boundary conditions for FE simulations. The weather data included dry bulb temperature, relative humidity, wind speed, global horizontal irradiance, and incident infrared radiation from the sky.

The experiment at the Charleston facility was designed to evaluate the thermal performance of TABE panels installed on walls. Four wall panel assemblies, one baseline and three TABE panels, were constructed. Figure 4 shows the constructed layout for each panel at the Charleston facility. The exterior surface of the panels consisted of exterior horizontal vinyl siding. Beneath the siding, two layers of 0.5 in. (1.3 cm) polyiso were used. The studs used in these panels were 2 × 4 studs spaced

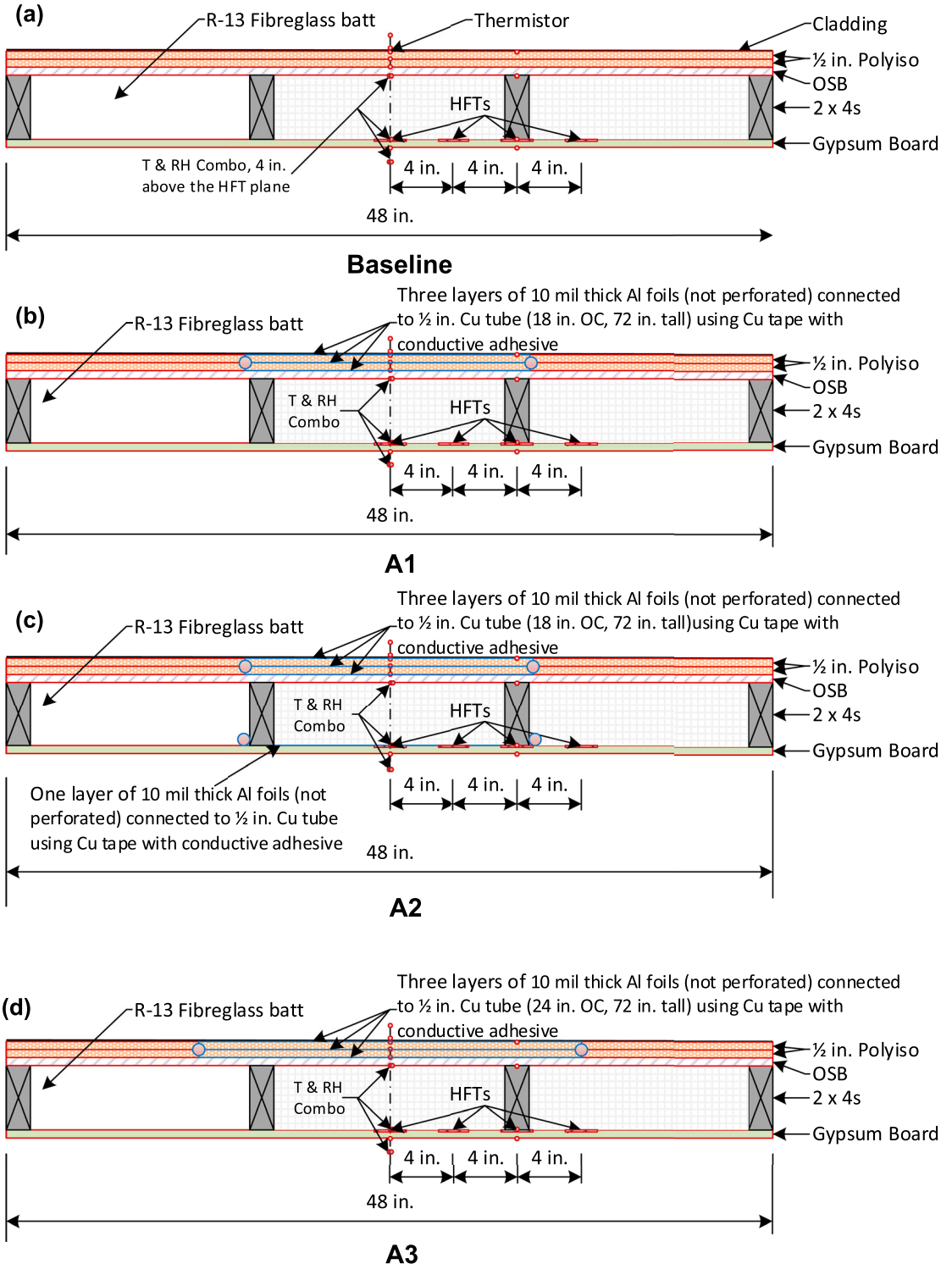


**Figure 4.** Cross sections of the TABE panels installed at the Charleston NET facility: (a) baseline, (b) A1, (c) A2, and (d) A3. HFTs 1, 2, 3, and 4 are numbered from left to right.

at 16 in. (0.41 m) in the centre. Between these studs, R-13 fibreglass batt cavity insulation was used. The innermost layer of the TABE panels consisted of 0.5 in. (1.3 cm) gypsum board. All wall panel assemblies met the International Energy Conservation Code (IECC) 2018 R-value requirements for residential building walls in climate zone 3.

All TABE panels (A1, A2, and A3) were constructed with three layers of aluminum foil. Like the RTRA roof panel foils, the selected foils were 10 mil (0.254 mm) thick.

**Table 1.** Reflectivity and emissivity of exterior cladding.

| | Solar reflectance (-) | Thermal emittance (-) |
|---|---|---|
| RTRA | 0.044 | 0.837 |
| Charleston | 0.505 | 0.881 |

These three foil layers were placed to sandwich all layers of polyiso in the construction. The foil layers were connected to 0.5 in. (1.27 cm) copper tubing via copper tape with conductive adhesive. The A2 panel had a fourth foil layer attached above the gypsum board. This fourth foil layer was connected to the internal hydronic loop as at RTRA. A1 and A3 were identical except for the spacing of the hydronic loop tubing. In the case of A1, the copper tubing was spaced at 18 in. (0.46 m). In the case of A3, the copper tubing was spaced at 24 in. (0.61 m). This allowed the evaluation of performance losses associated with larger spacing between TABE hydronic loops. In addition, 4 HFTs and 11 thermistors were used to monitor heat flux and temperature distribution at various locations on each panel. Thermistors were used to measure air temperatures adjacent to each panel. These thermistors protruded 3 in. (76 mm) from both the interior and exterior faces of each panel.

The plumbing system to control the TABE panels had a nearly identical design for both the RTRA and Charleston NET facility field evaluation sites. Figure 5 shows the plumbing system of the TABE panels at the Charleston facility, including the pipe layout and control system. This plumbing system includes three flow metres, eight water temperature sensors, three flow control valves, three manual valves, six solenoid valves, a reservoir, a chiller, a water tank, two pumps, and water pipes connecting them. The circulation of water in TABE started with a chiller that cooled the water temperature from a reservoir to the desired temperature. Then, the chilled water was pumped into a cold-water tank, which was used as the water source. Cold water stored in the tank was then pumped into TABE panels (i.e. A1, A2, and A3) for heat exchange. The outlet water was stored in the reservoir for heat dissipation and used as a water source for the chiller. The plumbing system of A1, A2, and A3 was independently controlled. For A1 and A3, only an exterior hydronic loop and the plumbing system were included. The system also included (1) the solenoid valve that turned the exterior hydronic loop on/off, (2) the flow control valve that controlled the water flow rate to the panels, (3) the thermocouples that measured the inlet and outlet water temperatures, and (4) the flow metre that measured the water flow rate. For A2, both the exterior and interior hydronic loops and a bypass loop were included. The inclusion of a bypass loop was important to ensure the plumbing system could be set to a desired water flow rate. The RTRA plumbing layout was identical except for the exclusion of the loop associated with A3. It should be noted that all experimental field testing relied on a chiller to maintain water temperature at the desired level. After initial field performance evaluations, further studies will be conducted using low-grade energy such as geothermal or integration with TES systems.

#### 2.1.2. Material property measurements

During construction of the TABE panels for field evaluations, thermal properties were measured for the primary insulative material layers. These measurements were necessary because the thermal conductivity of some materials used in the RTRA and Charleston facility panel constructions was temperature dependent. Therefore, experimental measurements were conducted to determine the thermal conductivity of the materials over a wide temperature range following ASTM C518 using a heat flow metre apparatus. Figure 6 presents the measured thermal conductivity as a function of temperature for TABE construction materials used for roofs at RTRA and walls at Charleston.

To correctly account for the effects of solar and infrared radiation, solar reflectance and thermal emittance were measured using solar spectrum reflectometers and emissometers (Table 1), respectively. These measurements were conducted for the RTRA's EPDM roof membrane and the Charleston facility's exterior cladding.

### 2.2. FE modelling

Modelling of active building envelopes presents significant challenges owing to dynamically adjustable thermal behaviour and complexity. Although passive building envelopes are dominated by one-dimensional heat transfer and a consistent thermal path, active building envelopes may employ heat redirection via two- or three-dimensional heat transfer paths. For TABE, capturing the full thermal performance characteristics precisely is important. Before the development of FE TABE models, various other methods were explored.

EnergyPlus, known for its capability of creating complex envelope assemblies, was initially considered. It has successfully demonstrated the potential in modelling a PCM-embedded envelope (Feng et al. 2022). However, EnergyPlus uses a one-dimensional heat transfer model with limited capability for handling complex, 3D heat transfer. Owing to TABE's 3D heat transfer, specifically the in-plane heat propagation along the conductive layers of TABE, this software was not selected as a solution for this application.

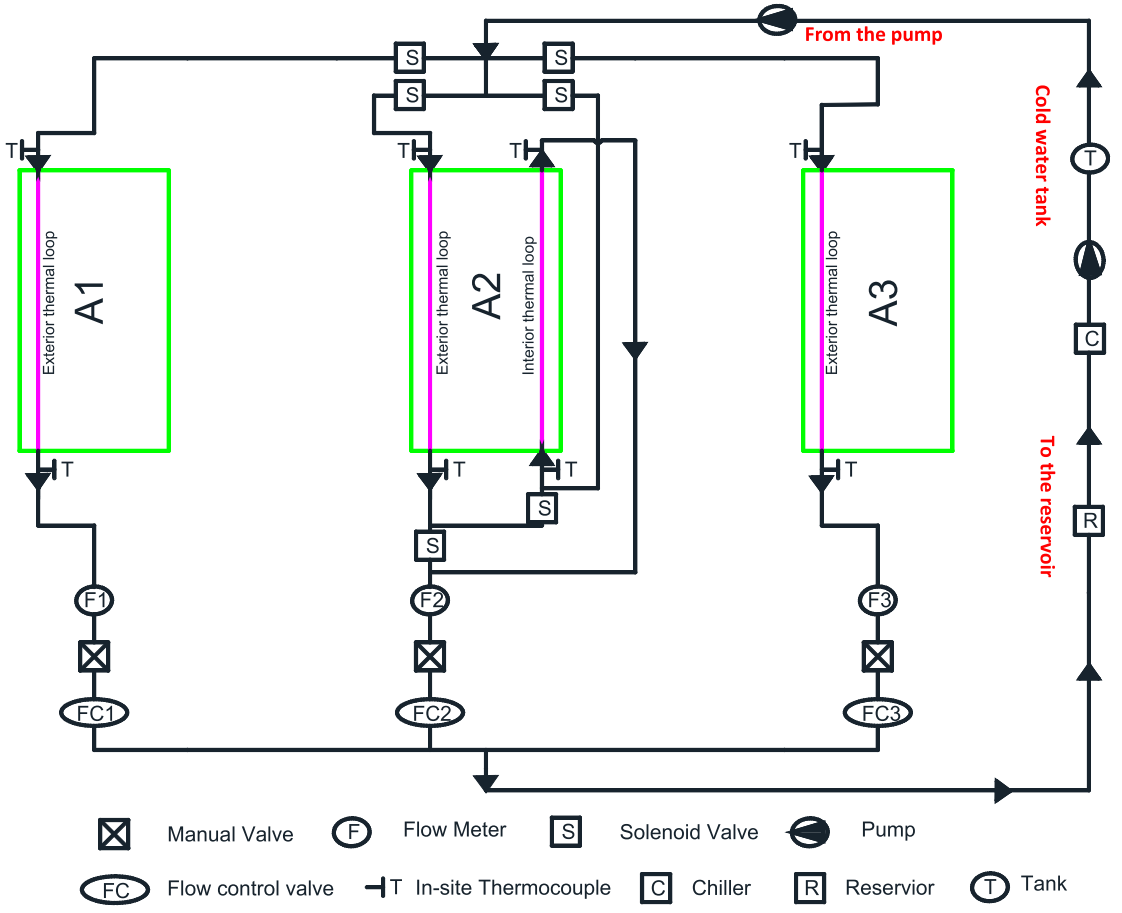


**Figure 5.** Plumbing system of TABE panels at the Charleston NET facility showing the pipe layout and control system.

A network of thermal resistors and capacitors, or RC model, has previously been used to develop complex active building envelope models, including hydronic systems. For example, Nestor Dias assessed the energy performance of integrating hydronic tubes into a ceiling application using the RC model (Dias 2011). In this study, the dispersion of thermal energy from the hydronic tubes was considered using a fin approximation. However, implementing this methodology for TABE modelling is a challenge owing to the difficulty of approximating a multilayer construction by a fin. Additionally, capturing the precise temperature and heat flux data at points at sensor locations of the field experimental setup would be impossible with this approximate model. Thus, FE modelling was chosen for developing the detailed TABE models. FE modelling has been previously used to investigate hydronic systems. For instance, Alghamdi used FE modelling to study hydronic systems combined with encapsulated PCM in a flooring application (Alghamdi 2024).

Unlike many previous FE models of hydronic and active envelope systems, the FE models created for the TABE analysis required use of real-world weather conditions as the boundary conditions for model calibration. Detailed FE models for the baseline (Figure 7**[a]**) and TABE panels (Figure 7**[b] and [c]**) at the Charleston facility and RTRA test sites were developed in COMSOL multiphysics. The detailed models contained all material layers and properties used in each experimental panel. Temperature-dependent thermal conductivities of each material were input into the FE models. Exterior and interior surface boundary conditions were applied based on outdoor temperature, solar radiation, infrared radiation, and indoor temperature. Data for these boundary conditions were obtained from each field test site and imported into the FE models.

To fully capture all heat transfer components associated with the TABE panels, multiple boundary conditions had to be applied to each panel surface to handle the various sources of convection and radiation for each respective case. A description of the equations used to assign each boundary condition follows.

The heat flux applied to the interior surface of the panel, $q_1$, is

$$q_1 = h_{int}(T_{int}^{air} - T_{int}^{surf}), \tag{1}$$

where $h_{int}$ is the film coefficient of the interior surface, which can be calculated by matching the modelled interior surface temperature ($T_{int}^{surf}$) with its experiment

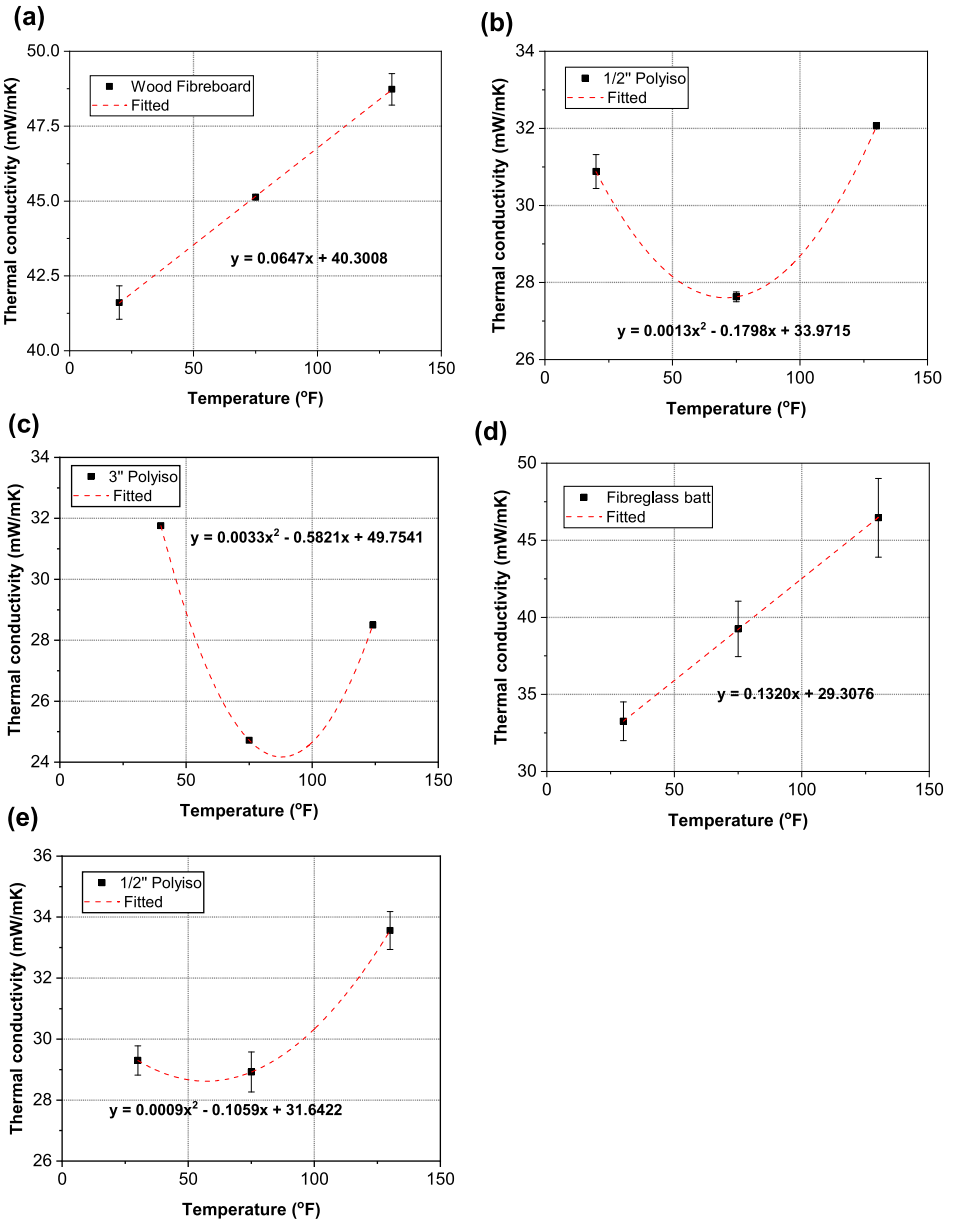


**Figure 6.** Thermal conductivity of materials as a function of temperature: (a) $\frac{1}{2}$ in. wood fibreboard at RTRA; (b) $\frac{1}{2}$ in. polyiso at RTRA; (c) 3 in. polyiso at RTRA; (d) fibreglass batt at Charleston; and (e) $\frac{1}{2}$ in. polyiso at Charleston.

counterpart; and $T_{int}^{air}$ is the indoor air temperature. The selected $h_{int}$ is the effective film coefficient, which includes various unknown effects, such as the radiation on the interior building surface and air velocity induced by the HVAC system. This parameter was verified to fall within ASHRAE accepted ranges for both wall and roof surfaces (ASHRAE 2017).

The convection heat flux applied to the exterior surface of the panel, $q_2$, is

$$q_2 = h_{int}(T_{ext}^{air} - T_{ext}^{surf}), \tag{2}$$

where $h_{ext}$ is the convection coefficient of the exterior surface, which is automatically calculated by COMSOL using inputs of ambient temperature, wind speed, atmospheric pressure, and humidity; $T_{ext}^{air}$ is the exterior (outdoor) air temperature; and $T_{ext}^{surf}$ is the exterior surface temperature of the panel.

For the exterior surface, the total radiation heat flux, $q_3$, includes the heat flux owing to solar radiation and infrared radiation; it can be calculated as

$$q_3 = q_{solar}(1 - S_r) + \varepsilon(q_{IR_{in}} - \sigma(T_{ext}^{surf})^4), \tag{3}$$

where $q_{solar}$ is the incident solar radiation on the building surface, $S_r$ is the solar reflectivity, $\varepsilon$ is the emissivity of the panel's exterior surface, $q_{IR_{in}}$ is the infrared radiation from the sky and ground, and $\sigma$ is the Stefan–Boltzmann

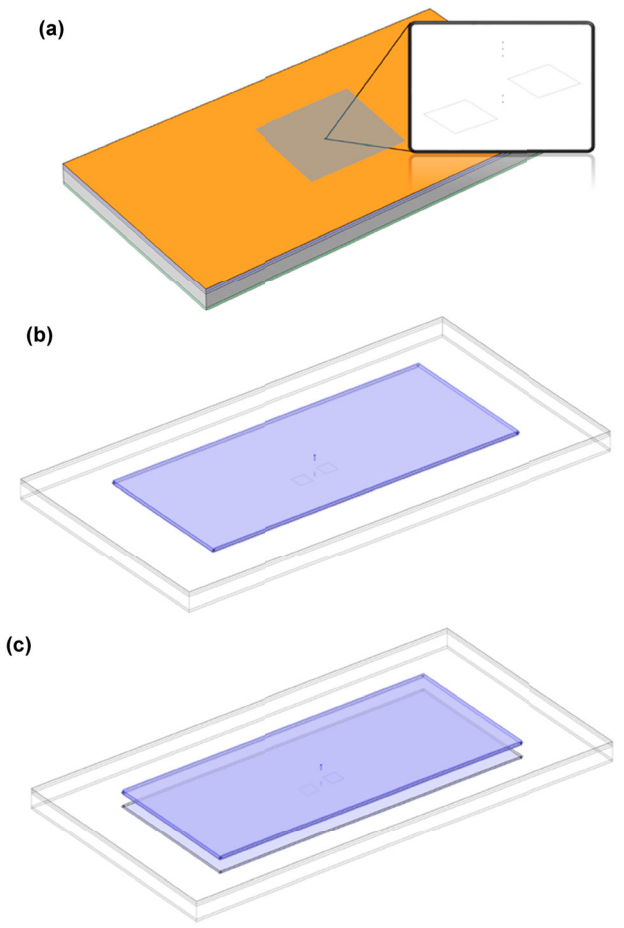


**Figure 7.** COMSOL FE models: (a) baseline panel at the RTRA with enlargement of temperature and heat flux sensors; (b) wireframe view of A1 at the RTRA showing three anisotropic layers and surrounding piping system; and (c) wireframe view of A2 at the RTRA showing one lower and three upper anisotropic layers and surrounding piping systems for interior and exterior loops.

constant. The values of $S_r$ and $\varepsilon$ are provided from experimental measurements conducted before panel construction. Some adjustments were made to $S_r$ because dust accumulation over time will affect the reflectivity of the surface.

In addition, the heat flux between the fluid in the pipe and the inner surface of the pipe, $q_{pipe}$, needs to be considered and can be calculated as

$$q_{pipe} = h_{pipe}(T_{water} - T_{int\_surf\_pipe}), \tag{4}$$

where $h_{pipe}$ is the convection coefficient between the water fluid and the inner surface of the pipe. It can be calculated by COMSOL based on an internal forced convection flow correlation derived from the pipe diameter (D) and fluid velocity (U). Also, $T_{int\_surf\_pipe}$ is the interior surface temperature of the pipe, and $T_{water}$ is the water temperature, which can be estimated as the average of the inlet and outlet water temperatures.

## 3. Results and discussions

Results at the RTRA and the Charleston NET facilities were evaluated to compare the simulated heat fluxes with their measured experimental counterparts. Additionally, comparisons were made with respect to heat flux savings from various anisotropic configurations on a test-specific basis (1 week test period) and on a total test period basis. Because field data was used to calibrate the FE models, some model modifications were necessary to more accurately capture the real-world heat transfer effects and sensor placements.

Moreover, sensitivity analysis was conducted for each of the adjusted parameters to demonstrate the effect of each on the mean square error (MSE) between the experimental and FE model heat flux. The mean square error was calculated for each test period and is given by

$$\text{MSE} = \frac{1}{N}\sum_{i=1}^{N}(f_i - y_i)^2, \tag{5}$$

where $N$ is the number of data points, $f_i$ is the value calculated by the model, and $y_i$ is the experimental value for data point $i$.

Figure 8 presents the MSE comparisons for the sensitivity study of the convergence threshold, surface solar reflectance. Setting a proper convergence threshold was critical to capture the time-dependent thermal effects of the TABE accurately. The convergence threshold for the simulation was controlled by the solver tolerances within the FE analysis environment. The default solver tolerances of COMSOL were insufficient to capture the transient heat flux with a 10 min resolution. Therefore, a smaller convergence threshold of $10^{-3}$ was imposed to ensure the transient heat fluxes were calculated accurately.

The solar reflectance on the exterior surface of the panels at the Charleston NET facility also had to be adjusted within the FE models. Although solar reflectance data were collected for these materials before field evaluation, some modification is required owing to uncertainty in the weathering of the material and in measurement of the solar irradiance on the panel surface. Solar reflectance values for the exterior surfaces of Charleston panel models were increased from 0.505 (measured) to 0.75 to achieve the best match between experimental and simulated data.

One of these modifications was to adjust the heat convection calculated on the interior of the piping surface. To model flow through the piping system, a defined continuous temperature was required on the interior of the piping surfaces. However, because the experimental pipe flow temperature sensors were located outside of the panel, these readings could not be used in the model during periods of no fluid flow. During periods of fluid flow,

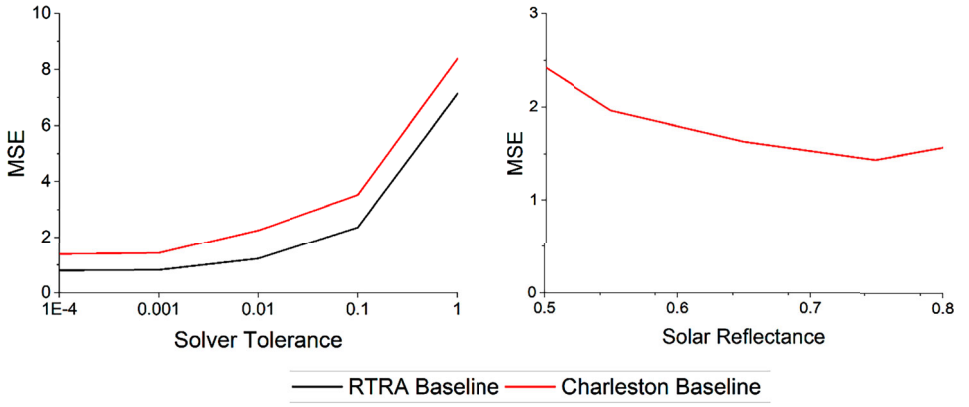


**Figure 8.** MSE between experimental and simulated wall panel heat fluxes: sensitivity to solver tolerance and solar reflectance.

the temperature measured by sensors outside of the TABE panel should be approximately identical to that at the beginning of the hydronic loops. In this small region of piping, the travelling fluid would not experience appreciable heat transfer. On the other hand, during periods of no fluid flow, the experimental sensors measured the temperature of the stationary fluid in the piping at the exterior surface of the panel. This temperature did not reflect the temperature inside the TABE panel, where the stationary fluid would quickly approach the surrounding piping surface temperature. This was addressed by using a condition to select temperature readings from experimental flow sensors during periods of flow and from simulation probes surrounding the pipe structure during periods of no flow. This setup effectively resulted in no convection occurring on the interior of the pipe surfaces during periods of no flow.

An additional model modification was made for the A2 panel model at the Charleston NET facility. The sensitivity of the distance parameters is shown in Figure 9. To align with the experimental heat flux, the HFT sensors in the FE model were positioned 0.1 in. (2.5 mm) away from the inner anisotropic layer surface. In the experimental setup, a small gap likely exists between the actual HFT sensors and the inner aluminum layer. This adjustment led to a substantial change in the heat flux results and allowed the model to effectively track the heat flux pattern observed in the experimental data.

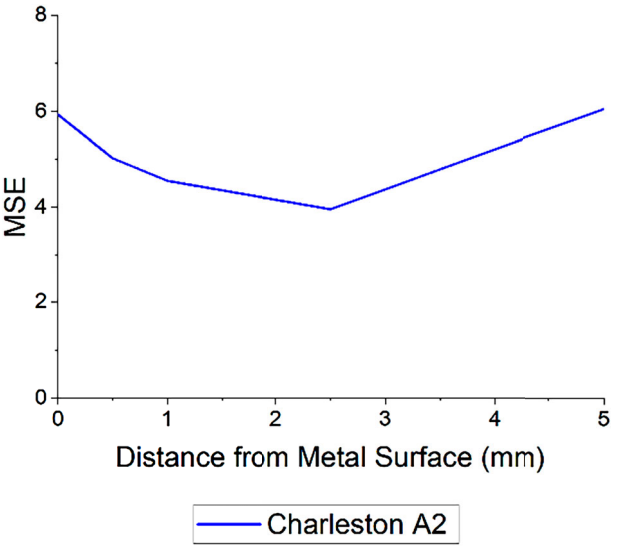


**Figure 9.** MSE between experimental and simulated wall panel heat fluxes: sensitivity of HFT proximity to the metal surface.

### 3.1. RTRA results

To understand performance of the TABE roof system under various operating conditions, specific testing periods were identified and are presented with their testing parameters in Table 2. Data from four summer weeks were used to test the performance of TABE considering the variations of water tank temperature, anisotropic loop used (for multi-loop configurations), and fluid flow rate through the panel piping systems. Additionally, the schedule for TABE use was varied to explore hours in which TABE would provide the most benefit.

The experimental and simulated interior and exterior surface temperatures are compared in Figure 10(a) for July 3–10, 2020. The exterior surface temperatures of the FEM model at the RTRA closely matched their corresponding field evaluation data and demonstrated that both solar and infrared radiations were applied correctly. These results are evidenced by the excellent match between the peak (afternoon) temperatures of each panel and the slight differences between the measured and simulated temperature peaks. The interior surface temperatures agreed well during most of the diurnal cycle but exhibited some systematic differences in the peak temperatures for all TABE panels. The peak daily interior surface temperature had a magnitude for all simulation results lower than that of those experimentally measured. This discrepancy is likely caused by radiation acting on the interior face of the building. No instrumentation was installed

**Table 2.** RTRA panel test matrix.

| Start date | Active loop[a] A2 | TABE on schedule (h) | Inlet water temp. (°C) | ID[b] temp. average (°C) | OD[c] temp. average (°C) | Flow rate ($10^{-5}$ $m^3/s$) |
|---|---|---|---|---|---|---|
| July 3, 2020 (Test 1) | Interior loop | 6–21 | 10 | 23.2 | 26.8 | 3.15 |
| July 21, 2020 (Test 2) | Interior loop | 6–21 | 15.6 | 23.3 | 26.5 | 3.15 |
| August 3, 2020 (Test 3) | Exterior loop | 6–21 | 15.6 | 23.3 | 25.5 | 3.15 |
| August 17, 2020 (Test 4) | Interior loop | 6–21 | 15.6 | 23.3 | 24.3 | 3.15 |

[a]Only the active loop of A2 was listed, and A1 follows the same schedule; [b]ID: indoor air; [c]OD = outdoor air

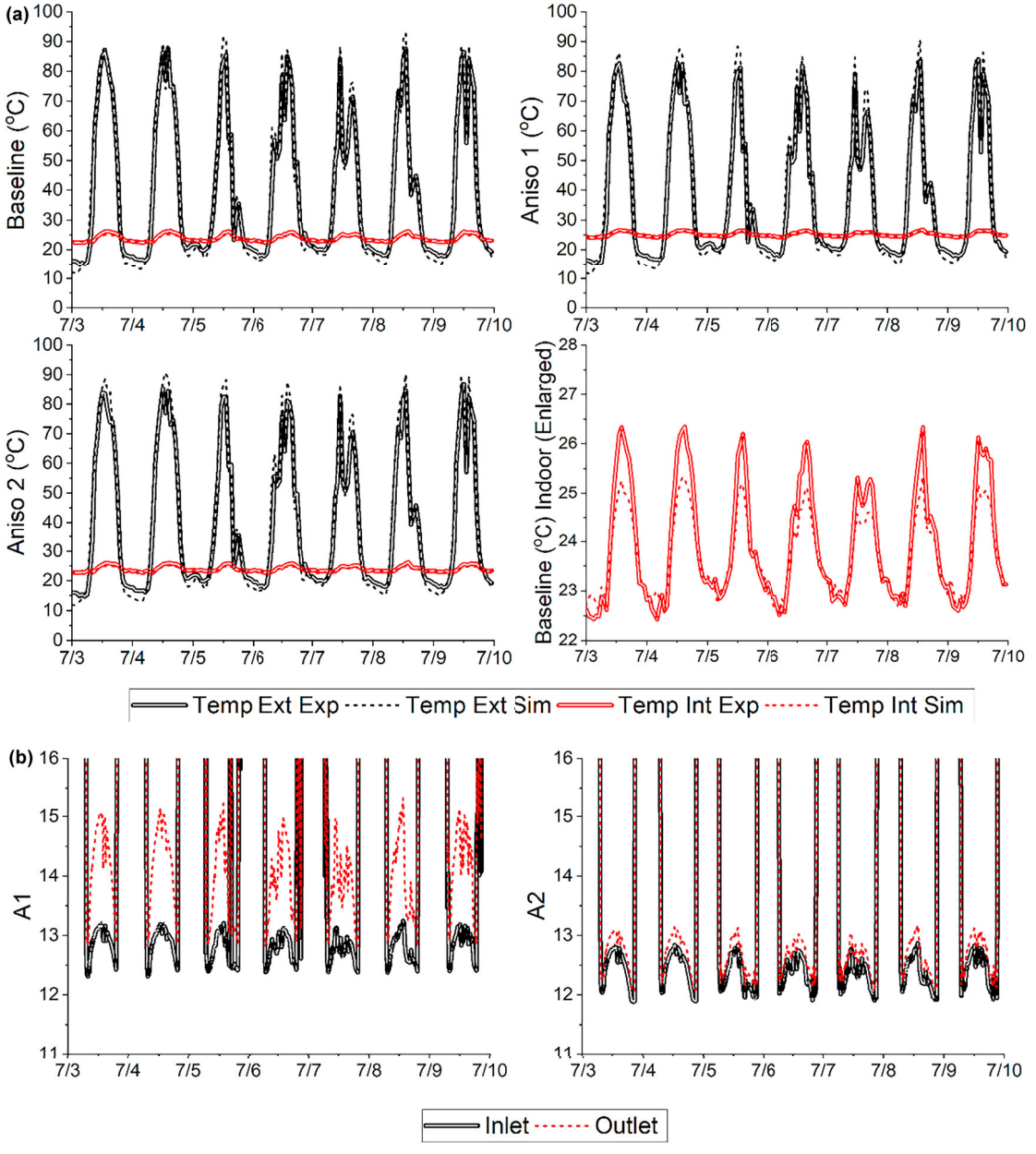


**Figure 10.** Experimental and simulated temperatures at the RTRA site for July 3–10, 2020: (a) roof panel surface temperatures and (b) measured inlet and outlet water temperatures.

in the experimental test to measure the radiation fluctuations on the interior panel surface. Numerous factors could have contributed to radiation changes on the interior panel surfaces, including lighting, equipment, and reflected solar radiation. Based on a reasonable boundary condition implementation, the heat flux comparison through the TABE demonstrated that conductive heat transfer was sufficiently accounted for throughout the

modelling of the TABE system. Figure 10(b) presents the measured water temperature for the same experiment period. Note that we presented the water temperatures only when the hydronic loops were activated, and temperatures outside of the *y*-axis limits are the times when the system has no water flow. When water flow is occurring in the TABE hydronic loops, the outlet water temperatures are consistently higher than those of the inlet, demonstrating the effective heat removal from the TABE roof via the water flow. As shown in the figure, the outlet water temperature of the A1 panel was significantly higher than that of the A2 panel. This is because during this time, the A2 panel used the interior hydronic loop, which is insulated from the environment and collects much less heat than the exterior loop of the A1 panel collects.

Heat flux comparisons are presented in Figure 11. HFT sensor 1 was excluded from the comparison because it had some contact with the metal sheathing, which led to a low signal-to-noise ratio compared with that of the other HFTs. Consistent patterning and magnitude between experimental and simulated data were observed. Figure 12 compares the total heat flux for each testing period. The discrepancies between experimental and simulated total heat flux likely resulted from variations in convection on the interior panel surface caused by nonuniform airflow because of the irregular placement of interior fans. The net accumulative heat flux was obtained by adding the heat flux of each test and is listed in Table 3. Again, the results show a good match with a maximum difference of 6.2% for A1.

Using the calibrated TABE roof model, the total heat flux was calculated for the selected periods with savings compared with the baseline roof panel, as shown in Figure 13. A1 has the largest savings, more than 80% for all the tests. Meanwhile, A2 has relatively smaller. The performance difference between A1 and A2 may have resulted from the discrepancy in interior surface temperatures between these two panels during some testing periods. Surprisingly, we did not find much influence of the inlet water temperature on the behaviour of heat flux savings. This may be because the large water flow rate in current tests is sufficient to remove heat if the water temperature is lower than a threshold (in this case, a threshold of 15.6°C).

### 3.2. Charleston facility results

Following the same process applied for the evaluation of RTRA panels, results for the NET facility were evaluated to compare experimental and FE model simulated heat flux data. Table 4 lists the testing periods and their specific testing parameters. It includes the start date for the weekly testing period, activated hydronic loop (interior or

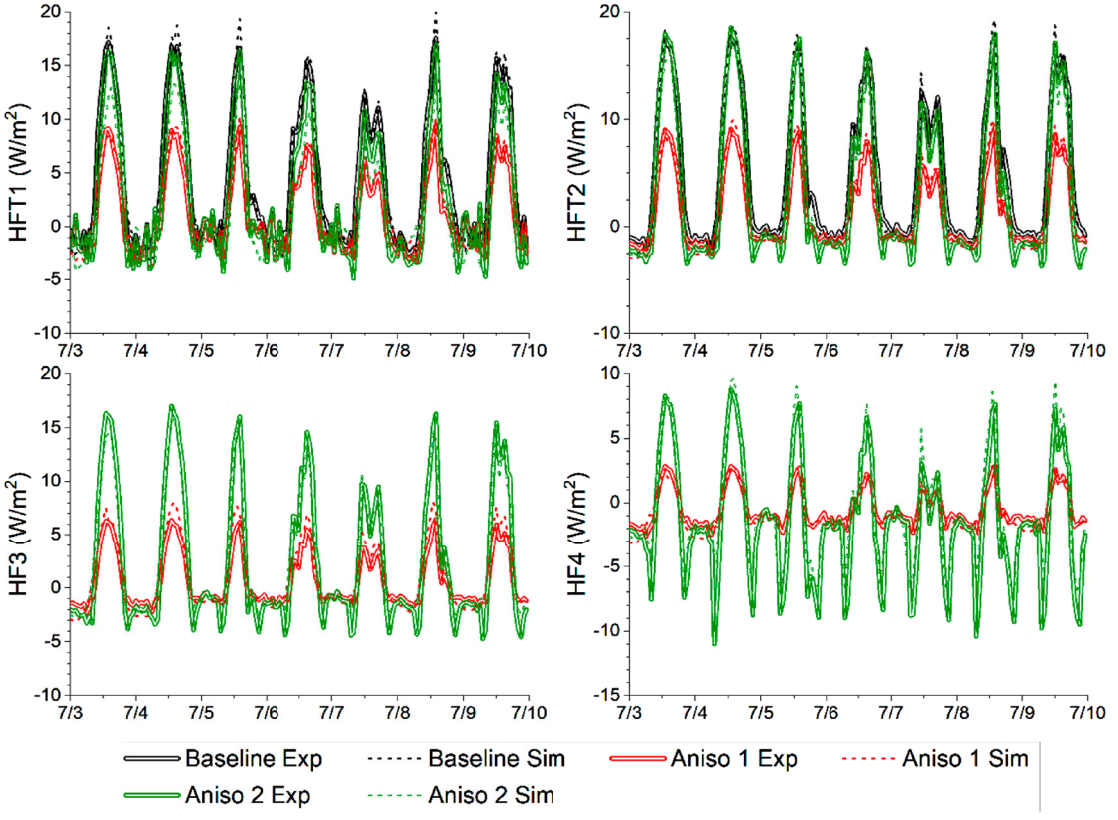


**Figure 11.** Experimental and simulated roof panel heat flux at the RTRA site for July 3–10, 2020.

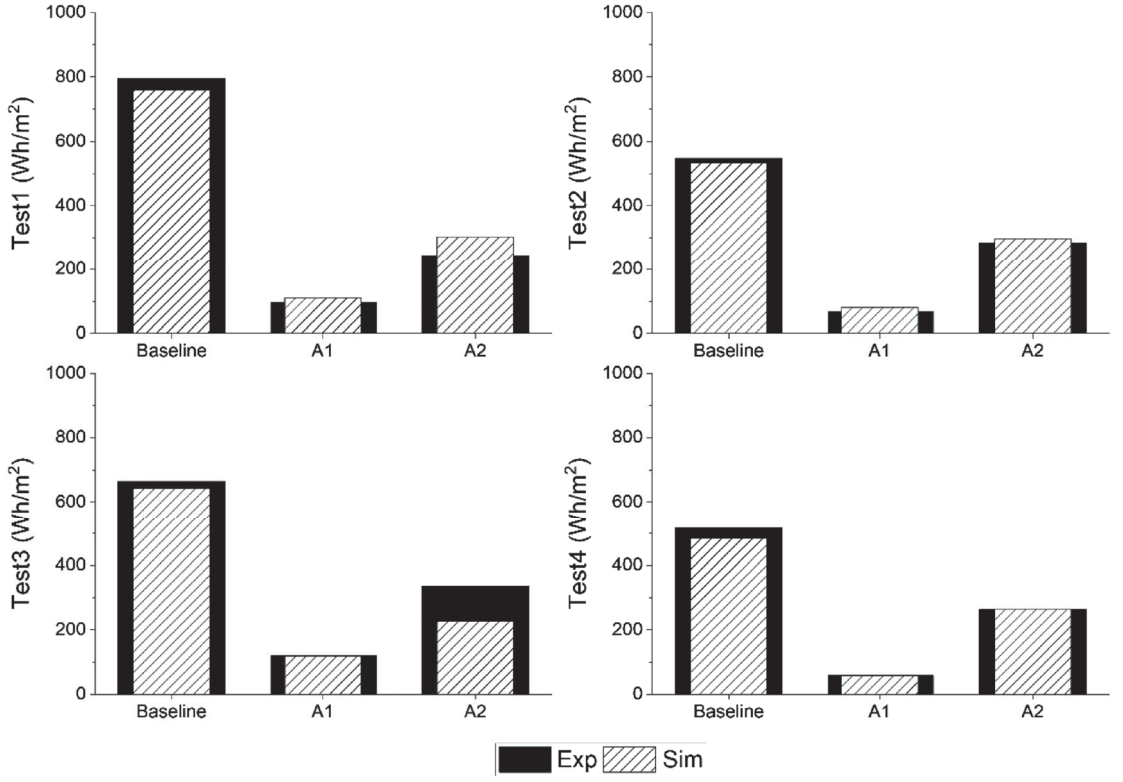


**Figure 12.** RTRA experimental vs. simulated cumulative heat flux for each testing period.

**Table 3.** Experimental and predicted cumulative net heat flux of RTRA roof panels during the evaluation periods.

| Panel | Cumulative net heat flux (Wh/m$^2$) | | Percent difference (%) | Mean square error |
|---|---|---|---|---|
| | Experimental | COMSOL | | |
| Baseline | 2,524 | 2,419 | −4.2 | 0.82 |
| A1 | 342 | 364 | 6.2 | 0.46 |
| A2 | 1,127 | 1,090 | −3.2 | 1.78 |

exterior), scheduled hours for TABE panel operation, temperature set point for the chilled fluid, average indoor and outdoor panel surface temperatures, and fluid flow rate through the TABE wall system.

Comparisons between experimental and simulated interior and exterior surface temperatures are shown in Figure 14(a). The exterior surface temperatures were compared to assess effectiveness of the imposed boundary conditions on the surface to model the experimental environment. Discrepancies between the experimental and simulated temperature data were observed and are primarily related to the deviation in the magnitude of the peak surface temperatures. Some of these discrepancies are likely attributed to shading from nearby trees at the Charleston facility. Trees casting shadows on the TABE panels would have a significant effect on radiation incident to the surface and, thus, peak temperature. Interior surface temperatures also showed some variations (particularly for A2), but they were relatively small. The inlet and outlet water temperatures of the same test periods are presented in Figure 14(b). Similarly, the outlet water temperatures of A1 and A3 panels were significantly higher than that of A2 panels owing to the use of its interior hydronic loop during this time.

Figure 15 compares the heat flux behaviour of the simulated data and their corresponding field evaluation counterparts. Overall, they matched very well (particularly in A2) and showed excellent agreement in magnitude. A small phase shift was observed for the baseline panel (HFT sensor 3), which likely results from the exterior radiation boundary conditions. As discussed earlier, this may be caused by shading effects. Cumulative heat flux for each testing period (Figure 16) shows that when running the exterior hydronic loop, the performance of A2 is comparable to that of A1 and A3 (Test 3). During the tests, a large cooling heat flux gain was achieved by using the interior hydronic loop of A2 for the summer weeks. HFT sensor 4 was excluded from the analysis because it was located outside the anisotropic region of the panel. Multiple factors may contribute to the anomalies in experimental heat flux data collected from this region, including the degree of thermal contact between the stud and the HFT. It was expected that the measured heat flux outside of the anisotropic region would experience large 3D heating effects emanating from the perimeter of each panel.

**Table 4.** Charleston facility panel test matrix.

| Begin date | Active loop[a] A2 | TABE on schedule (h) | Water temp. (°C) | ID[b] temp. average (°C) | OD[c] temp. average (°C) | Flow rate ($10^{-5}$ $m^3/s$) |
|---|---|---|---|---|---|---|
| June 30, 2020 (Test 1) | Interior loop | 6–21 | 10 | 22.6 | 28.6 | 2.52 |
| July 21, 2020 (Test 2) | Interior loop | 6–21 | 15.5 | 22.6 | 28.7 | 2.52 |
| August 3, 2020 (Test 3) | Exterior loop | 6–21 | 15.5 | 22.6 | 28.2 | 2.52 |
| August 17, 2020 (Test 4) | Interior loop | 6–21 | 15.5 | 22.7 | 26.4 | 2.52 |

[a]Only the active loop of A2 was listed, and A1 follows the same schedule; [b]ID: indoor air; [c]OD = outdoor air

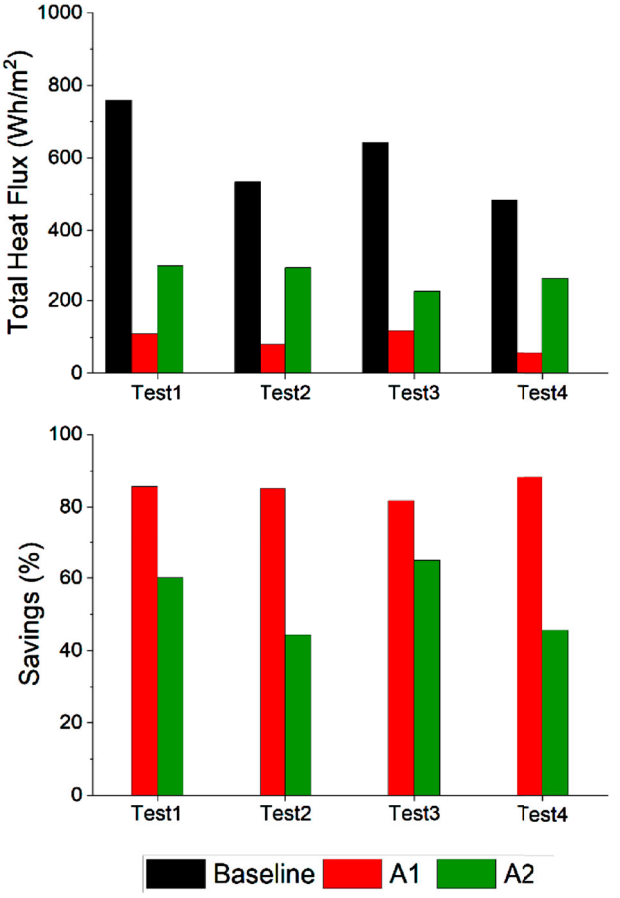


**Figure 13.** Predicted heat flux and savings during different test periods at the RTRA.

In modelling, these boundaries were assigned to be adiabatic because no data regarding heat transfer across these boundaries were collected.

Table 5 quantifies the cumulative net heat flux and the percentage difference between the experimental and simulated heat flux at the Charleston NET facility, along with the associated mean square error during the studied cooling weeks. The results show that the percentage difference in the cumulative net heat flux between them is less than 20%. As mentioned earlier, the difference is mainly due to the uncertain shading effects and the assumed adiabatic boundary condition along the perimeter of the panel. This adiabatic boundary condition had to be assumed because no data were collected regarding experimental heat flux in this region. In addition, the total heat flux and savings with respect to the baseline panel are presented in Figure 17. All the TABE panels led to significant thermal load reductions because of their ability to reverse the heat flux direction (indicated by the negative sign). Therefore, the weekly cooling load reduction of TABE will also be significant, which indicates its superior performance.

### 3.3. Discussions

The authors noticed that advanced model calibration techniques such as the Kennedy and O'Hagan method (Kennedy and O'Hagan 2001), ordinary least squares estimation, and Bayesian history matching are available (Sung and Tuo 2024). However, implementing these methods in complex FE models presents significant challenges. The FE models of the TABE panels require several hours of computation time to simulate each 1 week testing period, which is a considerable computational load. Given this computational expense, advanced methods become impractical owing to their high demand for computational resources and the complexity involved in their application.

Moreover, these advanced techniques often necessitate a high degree of precision in model setup and data quality, which can be difficult to achieve consistently in real-world scenarios. The intricate nature of the FE models, combined with the variability and potential errors in experimental data, complicates the calibration process. Additionally, the iterative nature of advanced calibration methods can lead to extensive computational cycles, further increasing the strain on time and resources.

Therefore, to balance accuracy and feasibility, we manually tuned the model parameters. The parameter tuning process was guided by observable trends and comparisons between the models and their experimental counterparts. By focusing on manual adjustments, we could directly address discrepancies and fine-tune the models more efficiently, thereby enabling us to account for real-time data variations and model behaviour nuances that might be overlooked by automated calibration techniques. Ultimately, this practical approach ensured that the FE models accurately

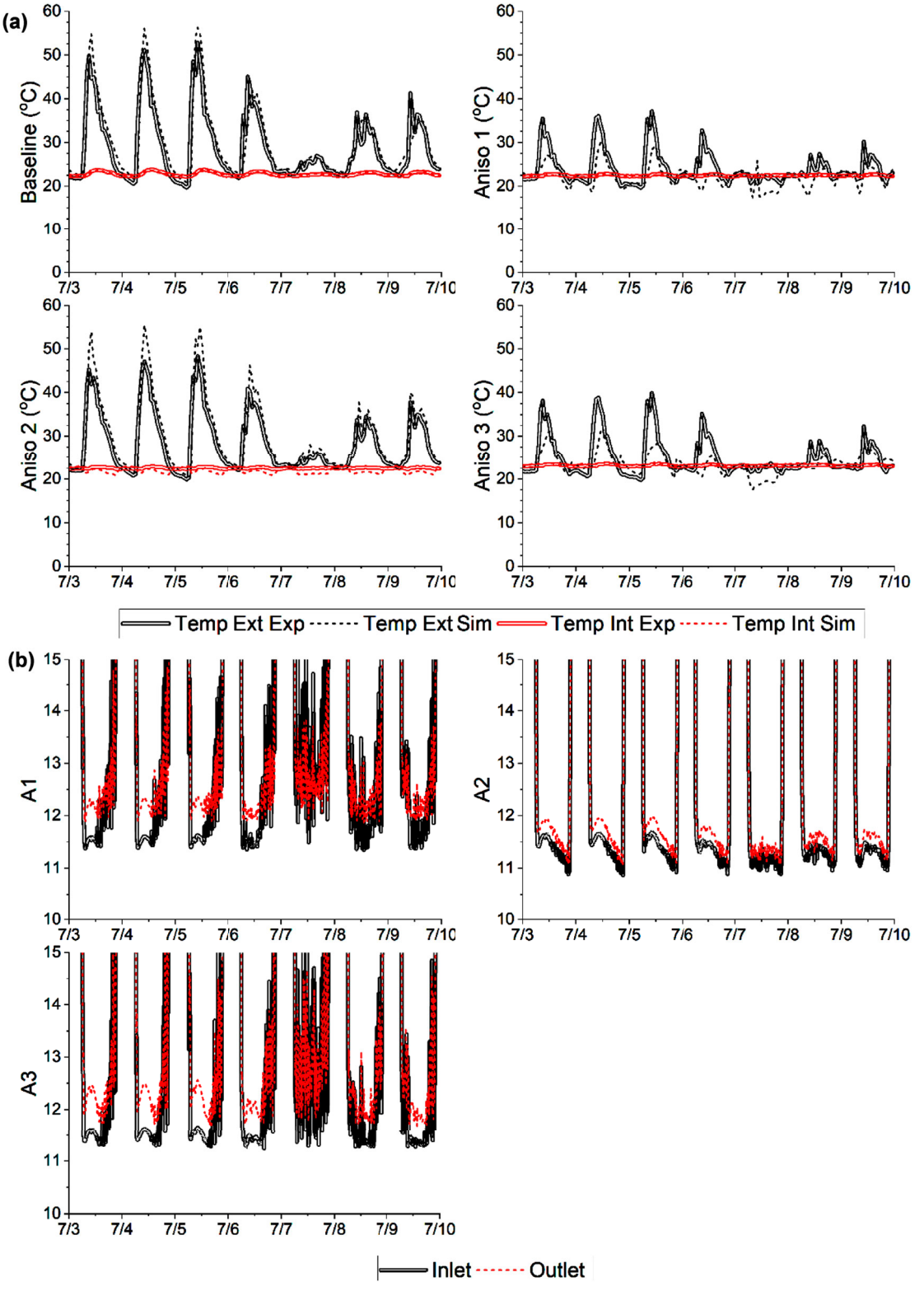


**Figure 14.** Experimental and simulated wall panel surface temperatures at the Charleston facility for July 3–10, 2020.

represented the real-world behaviour of the TABE panels while remaining computationally manageable.

Building on previous work with FE modelling of hydronic systems, the TABE models created for this analysis used real-world weather data to develop the boundary conditions. These detailed FE models also allowed for location-specific data corresponding to the placement of temperature and heat flux sensors in the experimental setup. Owing to the incorporation of these complex details, multiple adjustments were required to

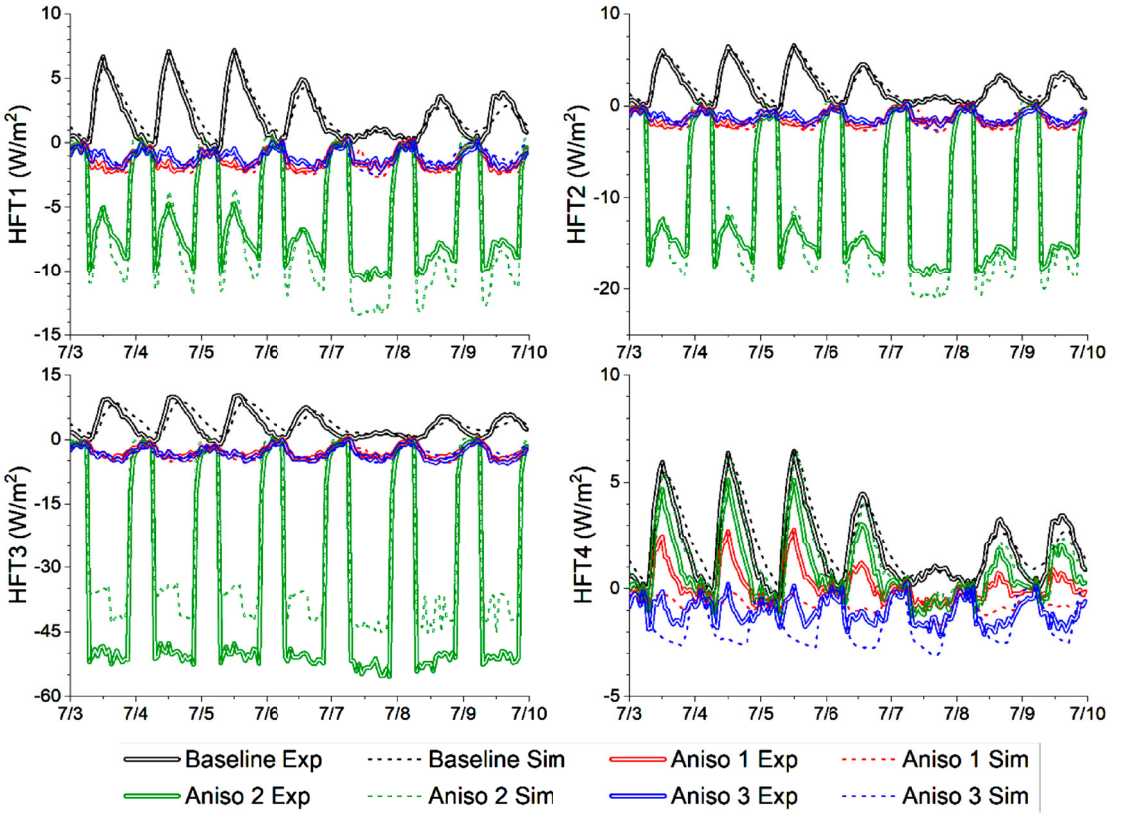


**Figure 15.** Experimental and simulated heat flux of the Charleston facility wall panels.

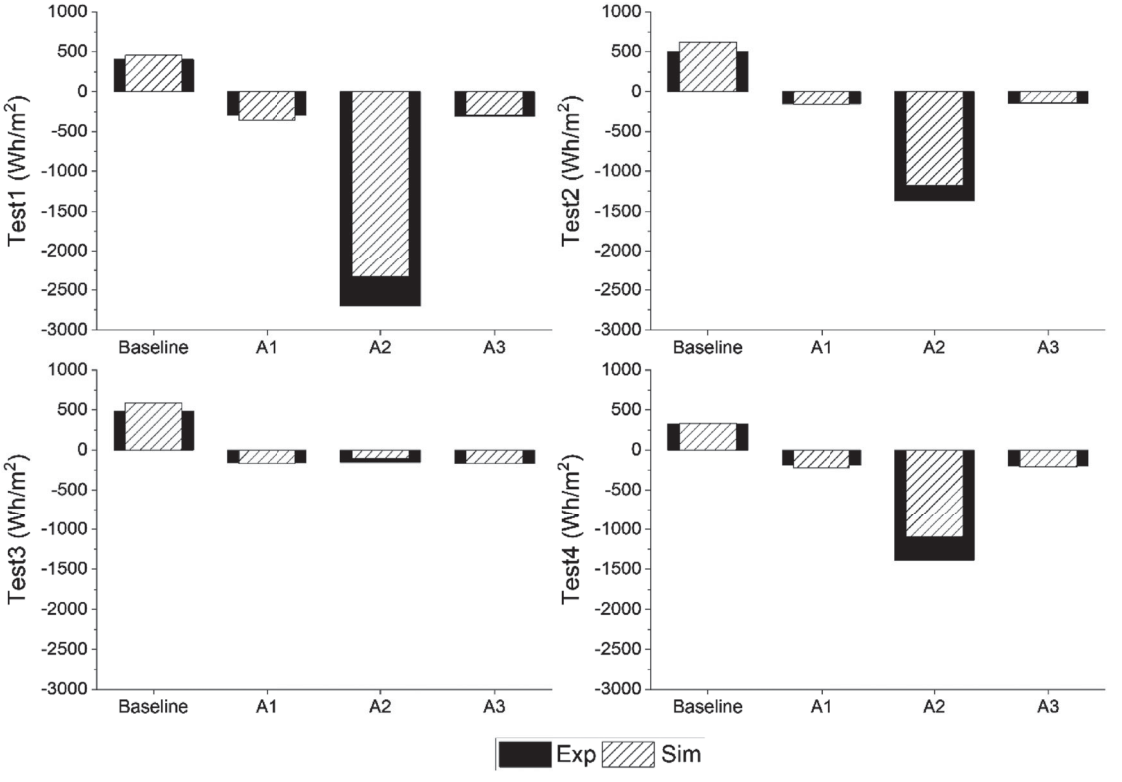


**Figure 16.** Charleston facility experimental vs. simulated cumulative heat flux for each testing period.

**Table 5.** Experimental and predicted cumulative net heat flux of the Charleston facility wall panels during the evaluation periods.

| Panel | Cumulative net heat flux (Wh/m$^2$) | | Percentage difference (%) | Mean square error |
|---|---|---|---|---|
| | Experimental | COMSOL | | |
| Baseline | 1,706 | 2,001 | 17.3 | 1.43 |
| A1 | −788 | −900 | 14.2 | 0.27 |
| A2 | −5,603 | −4,694 | −16.2 | 3.96 |
| A3 | −817 | −809 | −0.9 | 0.26 |

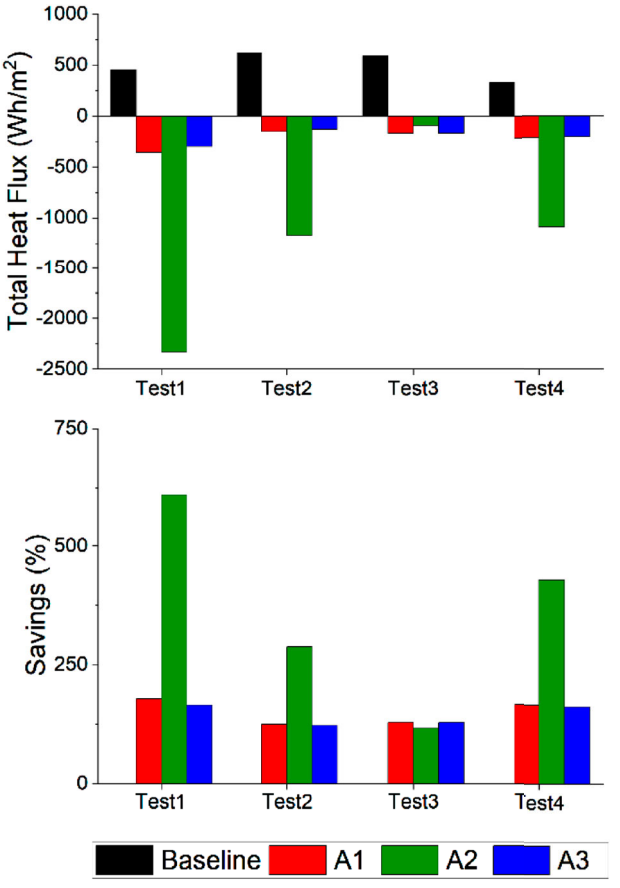


**Figure 17.** Predicted heat flux and savings during different test periods at the Charleston facility.

parameters and techniques to capture all heat transfer physics of the experimental counterpart.

Properly assigning boundary conditions was important to address the heat flux phase shift observed in modelling. For example, the Charleston facility models showed a considerable amount of phase shift between the experimental and simulation heat fluxes (see Figure 16). To determine the potential causes of such a phase shift, several simulation cases were conducted. First, simulations were conducted with explicitly defined interior and exterior surface temperatures (per experimental data), and there was no observed phase shift. This phase shift was also not apparent when using the measured exterior surface temperature and only applying convection and radiation boundary conditions to the interior surface. This indicated that the phase shift resulted from the imposed convection and radiation boundary conditions on the exterior panel surfaces. Both solar radiation and exterior convection were independently validated against EnergyPlus outputs and showed no discrepancy. The incoming infrared radiation then was determined as the cause of this phase shift. Because no data regarding ground temperatures were available from the Charleston facility, infrared radiation exchange between the exterior surface and the ground was neglected.

Excellent agreement between the experimental and simulated heat flux was obtained for both the TABE roof panel at RTRA and the TABE wall panel at the Charleston facility. Large thermal load reductions were achieved by using the TABE system. At the Charleston facility, the TABE system did not just reduce the thermal load—it reversed the load entirely. This means that the building envelope wall areas containing TABE panels could effectively be used to supplement a portion of HVAC demand because of the negative thermal load impact. On the other hand, the roof applications of TABE panels were not able to reverse the heat flux direction because of the much larger thermal loads (from larger solar radiation exposure) present in roofing configurations. Achieving heat flux reversal in roofing configurations like that of wall configurations would require increasing the TABE system's capacity for heat redirection. This could be achieved by using lower inlet fluid temperatures or by increasing the piping (heat sink) density throughout the TABE panels.

## 4. Conclusions

In this study, FE models of TABE roof and wall panels were calibrated using field evaluation data. Furthermore, the thermal load reduction potentials of TABE panels were quantified to evaluate performance. The following conclusions can be drawn:

(1) To achieve a high degree of accuracy from the calibrated FE models, multiple modifications were necessary during the calibration process. Adjustment to convergence tolerance, hydronic loop convection calculation, aluminum foil connectivity, and model sensory placement were all critical contributors in achieving the excellent agreement between the TABE models and their experimental counterparts.
(2) The surface temperature and heat flux of TABE predicted by the FE models match well with the experimental data following adjustments made during the

calibration process. The average percentage difference between the experimental and FE modelled heat fluxes was found to be −0.42% for roof panels and 3.57% for wall panels.

(3) Compared with the baseline panel, TABE panels demonstrated a massive reduction in heat flux penetration through the envelope and, therefore, a reduction in the associated thermal load. For the roof panels, heat flux reduction was up to 85% of the thermal load. Wall panels were capable not just of heat flux reduction; the panels entirely reversed the direction of heat flux. TABE roof and wall panel load reductions both allowed for significant reductions to building HVAC loads.

(4) The hydronic loop control strategy has a substantial effect on TABE roof and wall panels. When the exterior loop is active, the thermal load reduction potential is not highly dependent on the water flow rate. This is because TABE (in this operating condition) effectively acts as an insulation that separates the outdoor environment from the indoor environment. On the other hand, when the interior loop of TABE is active, larger water flow rates correlate to higher thermal load reductions. In this operation mode, TABE is directly utilized as a radiant heating/cooling system.

(5) Compared with TABE wall panels, TABE roof panels show a smaller reduction in heat flux. This is likely due to high solar radiation heat gain overwhelming the capability for TABE to redirect the heat.

The calibrated TABE FE models can be applied in different future research, such as the following:

- Layout optimization of the TABE roof to achieve thermal load reduction similar to that of the TABE wall. The current TABE roof layout is not sufficient to reduce the high thermal loads from solar radiation.
- Whole-building energy simulation to predict the energy-saving potential of TABE when applied in different climate zones and building types.
- Use of low-grade energy sources, such as geothermal or TES devices, to supply the heating/cooling energy in the hydronic loops.
- Integration of the thermal loads redistributed by the TABE with a TES system to store heating energy in the daytime for indoor heating in the nighttime or to store cooling energy in the nighttime for indoor cooling in the daytime.

## Acknowledgements

This research used resources at the Building Technologies Research and Integration Center, a DOE Office of Science User Facility operated by Oak Ridge National Laboratory. The authors would like to acknowledge Mr. Sven Mumme, Technology Manager, DOE Building Technologies Office, for his guidance. The authors thank Jerald Atchley and Anthony Gehl for the experimental setup and Olivia Shafer and Wendy Hames for formatting and technical editing.

## Disclosure statement

No potential conflict of interest was reported by the author(s).

## Funding

This work was supported by U.S. Department of Energy: [Grant Number].

## Data availability statement

The data that support the findings of this study are available from the corresponding author, S. S. S., upon reasonable request.

## References

Alghamdi, A. A. 2024. "Multiscale Finite Element Modeling of the Effect of Macro-Encapsulated Phase-Change Materials on the Thermal Performance of Hydronic Floor Heating Systems." *Buildings* 14 (3): 644. https://doi.org/10.3390/buildings14030644.

American Society of Heating, Refrigerating and Air-Conditioning Engineers. 2017. *ASHRAE Handbook: Fundamentals, 749*. Atlanta, GA: American Society of Heating, Refrigeration and Air-Conditioning Engineers.

Baetens, R., B. P. Jelle, and A. Gustavsen. 2011. "Aerogel Insulation for Building Applications: A State-of-the-Art Review." *Energy and Buildings* 43 (4): 761–769. https://doi.org/10.1016/j.enbuild.2010.12.012.

Baetens, R., B. P. Jelle, J. V. Thue, M. J. Tenpierik, S. Grynning, S. Uvslokk, and A. Gustavsen. 2010. "Vacuum Insulation Panels for Building Applications: A Review and Beyond." *Energy and Buildings* 42 (2): 147–172. https://doi.org/10.1016/j.enbuild.2009.09.005.

Bhamare, D. K., M. K. Rathod, and J. Banerjee. 2019. "Passive Cooling Techniques for Building and Their Applicability in Different Climatic Zones-The State of Art." *Energy and Buildings* 198:467–490. https://doi.org/10.1016/j.enbuild.2019.06.023.

Biswas, K. 2018. "Development and Validation of Numerical Models for Evaluation of Foam-Vacuum Insulation Panel Composite Boards, Including Edge Effects." *Energies* 11 (9): 2228. https://doi.org/10.3390/en11092228.

Biswas, K., S. Shrestha, D. Hun, and J. Atchley. 2019. "Thermally Anisotropic Composites for Improving Energy Efficiency of Building Envelopes." *Energies* 12 (19): 3783. https://doi.org/10.3390/en12193783.

Biswas, K., Y. Shukla, A. Desjarlais, and R. Rawal. 2018. "Thermal Characterization of Full-scale PCM Products and Numerical Simulations, Including Hysteresis, to Evaluate Energy Impacts in an Envelope Application." *Applied Thermal Engineering* 138:501–512. https://doi.org/10.1016/j.applthermaleng.2018.04.090.

Carpenter, J., P. Mago, R. Luck, and H. Cho. 2014. "Passive Energy Management through Increased Thermal Capacitance."

*Energy and Buildings* 75:465–471. https://doi.org/10.1016/j.enbuild.2014.02.044.

Cometto, O., M. K. Samani, B. Liu, S. X. Sun, S. H. Tsang, J. Liu, K. Zhou, and E. H. T. Teo. 2017. "Control of Nanoplane Orientation in voBN for High Thermal Anisotropy in a Dielectric Thin Film: A New Solution for Thermal Hotspot Mitigation in Electronics." *ACS Applied Materials & Interfaces* 9 (8): 7456–7464. https://doi.org/10.1021/acsami.6b15014.

Dias, F. 2011. "Modeling of a Hydronic Ceiling System and its Environment as Energetic Auditing Tool." *Applied Energy* 88 (3): 636–649.

Elnaijar, E. 2017. "Using PCM Embedded in Building Material for Thermal Management: Performance Assessment Study." *Energy and Buildings* 151:28–34. https://doi.org/10.1016/j.enbuild.2017.06.010.

Feng, F., Y. Fu, Z. Yang, and Z. O'Neill. 2022. "Enhancement of Phase Change Material Hysteresis Model: A Case Study of Modeling Building Envelope in EnergyPlus." *Energy and Buildings* 276: 112511. https://doi.org/10.1016/j.enbuild.2022.112511.

Hirmiz, R., H. Teamah, M. Lightstone, and J. Cotton. 2019. "Performance of Heat Pump Integrated Phase Change Material Thermal Storage for Electric Load Shifting in Building Demand Side Management." *Energy and Buildings* 190:103–118. https://doi.org/10.1016/j.enbuild.2019.02.026.

Huang, S. R., J. Bao, H. Ye, N. Wang, G. J. Yuan, W. Ke, D. S. Zhang, et al. 2016. "The Effects of Graphene-Based Films as Heat Spreaders for Thermal Management in Electronic Packaging." *17th International Conference on Electronic Packaging Technology*, 889–892.

Kennedy, M. C., and A. O'Hagan. 2001. "Bayesian Calibration of Computer Models." *Journal of the Royal Statistical Society: Series B* 63 (3): 425–464. https://doi.org/10.1111/1467-9868.00294.

Kosny, J., A. Fallahi, N. Shukla, E. Kossecka, and R. Ahbari. 2014. "Thermal Load Mitigation and Passive Cooling in Residential Attics Containing PCM-enhanced Insulations." *Solar Energy* 108:164–177. https://doi.org/10.1016/j.solener.2014.05.007.

Kosny, J., T. Stovall, S. Shrestha, and D. Yarbrough. 2010. "Theoretical and Experimental Thermal Performance Analysis of Complex Thermal Storage Membrane Containing Bio-Based Phase Change Material (PCM)." *Thermal Performance of the Exterior Envelopes of Whole Buildings XI International Conference* 7–8.

Lakhdari, Y., S. Chikh, and A. Campo. 2020. "Analysis of the Thermal Response of a Dual Phase Change Material Embedded in a Multi-Layered Building Envelope." *Applied Thermal Engineering* 179:1–13. https://doi.org/10.1016/j.applthermaleng.2020.115502.

Mokhtari, R., G. Ulpiani, and R. Ghasempour. 2022. "The Cooling Station: Combining Hydronic Radiant Cooling and Daytime Radiative Cooling for Urban Shelters." *Applied Thermal Engineering* 211: 118493. https://doi.org/10.1016/j.applthermaleng.2022.118493.

Pasupathy, A., and R. Velraj. 2008. "Effect of Double Layer Phase Change Material in Building Roof for Year Round Thermal Management." *Energy and Buildings* 40 (3): 193–203. https://doi.org/10.1016/j.enbuild.2007.02.016.

Ren, Z. Q., and J. Lee. 2018. "Thermal Conductivity Anisotropy in Holey Silicon Nanostructures and its Impact on Thermoelectric Cooling." *Nanotechnology* 29 (4): 45404. https://doi.org/10.1088/1361-6528/aa9f07.

Sadineni, S. B., S. Madala, and R. F. Boehm. 2011. "Passive Building Energy Savings: A Review of Building Envelope Components." *Renewable Sustainable Energy Reviews* 15 (8): 3617–3631. https://doi.org/10.1016/j.rser.2011.07.014.

Saffari, M., C. Roe, and D. Finn. 2022. "Improving the Building Energy Flexibility using PCM-Enhanced Envelopes." *Applied Thermal Engineering* 217:1–18. https://doi.org/10.1016/j.applthermaleng.2022.119092.

Sung, C. L., and R. Tuo. 2024. "A Review on Computer Model Calibration." *WIREs Computational Statistics* 16 (1): e1645. https://doi.org/10.1002/wics.1645.

Suszko, A., and M. S. El-Genk. 2016. "Thermally Anisotropic Composite Heat Spreaders for Enhanced Thermal Management of High-performance Microprocessors." *International Journal of Thermal Sciences* 100:213–228. https://doi.org/10.1016/j.ijthermalsci.2015.09.018.

Tarumi, H., S. Fujii, and N. Ito. 1991. "Conversion of Exhaust Heat to Latent Heat for the Management of the Thermal Environment in Urban Areas." *Energy and Buildings* 16 (1–2): 609–616. https://doi.org/10.1016/0378-7788(91)90029-3.

Termentzidis, K. 2018. "Thermal Conductivity Anisotropy in Nanostructures and Nanostructured Materials." *Journal of Physics D-Applied Physics* 51 (9): 94003. https://doi.org/10.1088/1361-6463/aaa82e.

Xing, D., and N. Li. 2022. "Reconstruction of Hydronic Radiant Cooling Panels: Conceptual Design and Numerical Simulation." *Thermal Science and Engineering Progress* 30: 101272. https://doi.org/10.1016/j.tsep.2022.101272.

Yang, L., H. Yan, and J. C. Lam. 2014. "Thermal Comfort and Building Energy Consumption Implications–A Review." *Applied Energy* 115:164–173. https://doi.org/10.1016/j.apenergy.2013.10.062.